Parallel kinematic mechanisms for distributed actuation of future structures

2016 J. Phys.: Conf. Ser. 744 012169

(http://iopscience.iop.org/1742-6596/744/1/012169)

Parallel kinematic mechanisms for distributed actuation of future structures

G Lai, A R Plummer, D J Cleaver and H Zhou

Centre for Power Transmission and Motion Control
Department of Mechanical Engineering
University of Bath, UK

E-mail: g.lai@bath.ac.uk

Abstract. Future machines will require distributed actuation integrated with load-bearing structures, so that they are lighter, move faster, use less energy, and are more adaptable. Good examples are shape-changing aircraft wings which can adapt precisely to the ideal aerodynamic form for current flying conditions, and light but powerful robotic manipulators which can interact safely with human co-workers. A 'tensegrity structure' is a good candidate for this application due to its potentially excellent stiffness and strength-to-weight ratio and a multi-element structure into which actuators could be embedded. This paper presents results of an analysis of an example practical actuated tensegrity structure consisting of 3 'unit cells'. A numerical method is used to determine the stability of the structure with varying actuator length, showing how four actuators can be used to control movement in three degrees of freedom as well as simultaneously maintaining the structural pre-load. An experimental prototype has been built, in which 4 pneumatic artificial muscles (PAMs) are embedded in one unit cell. The PAMs are controlled antagonistically, by high speed switching of on-off valves, to achieve control of position and structure pre-load. Experimental and simulation results are presented, and future prospects for the approach are discussed.

1. Introduction

Highly efficient aircraft are desirable for both environmental and economic reasons. A possible solution to further improve efficiency is to allow an aircraft to adapt its aerodynamic shape for different flight regimes. It is not a new concept to change the shape of an aerial vehicle. It can be dated back to the first powered and controlled aircraft which used a wing-warping system to change the twist of the wing [1, 2]. Modern commercial aircraft have already adopted active shape-changing devices in several components, e.g. leading-edge slats. Nevertheless, these are only effective for a limited part of the flight regime. A significant disadvantage of these devices is that they could result in the loss of lift or cause regional stall as the hinged connections create discontinuous surfaces [3].

It is believed that, for the next generation of aircraft, the actuation system and the structure should be tightly integrated together so as to allow the structure to change its shape while being capable of carrying aerodynamic loads [3]. It can thus reduce discontinuous surfaces and sharp edges of an aircraft. This requires actuators to be distributed within the structure. With the advent of 'smart' materials, e.g. shape memory polymer (SMP), elastic memory composite (EMC), etc., this target becomes more achievable, as these materials are not only deformable but also load-bearing [4]. Gern et al. conducted a computational study of actuation for smart wings [5]. The research shows that distributed actuation

for a morphing wing could provide a very robust and redundant actuation system avoiding the need for a complete backup system for each individual actuator as found in conventional aircraft. NASA also indicates that there will be no conventional mechanical connected parts in the future aircraft wing. It will be built of integrated, embedded "smart" materials and actuators to achieve superior aerodynamic efficiencies and aircraft control [6].

A tensegrity structure is a potential candidate for this future integration due to its unique properties. In fact, many organisms in the natural world, under natural selection, have already evolved tensegrity structures in their bodies because it is one of the optimum types of structure, e.g. human bones held by muscles and tendons [7]. The structure was first investigated by Emmerich, Fuller and Snelson in 1950s [8], and was named by Fuller who created the word tensegrity through the truncation of the phrase "tensional integrity" [9]. It is a multi-element structure with rigid members (struts) always in compression and flexible members (cables) always in tension. As its name suggests, the whole structure is required for 'integrity', and can only be stabilised by the tensile member forces acting on the compressive struts. There is no bending moment in any member or torque at any joint. Figure 1 is an example of tensegrity structure that has been built at the University of Bath. This is a class 3 structure as a maximum of 3 struts meet at a point.

Oliveira and Mauricio explain how a tensegrity structure can be reshaped by changing its balanced state [10]. Skelton et al. presented detailed illustrations of the advantages of tensegrity structures in their work, e.g. to facilitate high precision control, and promote the integration of structure and control disciplines [11]. Hence, by applying the knowledge of parallel kinematics, the structure may achieve good stiffness-to-mass ratio without sacrificing the number of degrees of freedom. Tensegrity structures have been suggested for aerospace (particularly space) application [8, 12-14] because they are lightweight and could be stowed and deployed easily [15]. Tensegrity structures have also been found to be good models of biological structures [16-18]. Researchers have developed different form-finding methods to analytically and numerically determine the pre-stressed level and its corresponding geometric configuration. Analytical methods [19-21] have been used to study tensegrities of relatively simple configuration (less nodes and elements) and tensegrities with high level of symmetry. Numerical methods [22-24] have been used for the study of more complicated tensegrities.

In this paper, the static state configuration of the proposed tensegrity structure is found by using an iterative approach as shown in Section 2. The experimental setup is presented in Section 3. A physical prototype with 1 unit cell of the proposed tensegrity was built. The unit cell is actuated by pneumatic artificial muscles (PAMs) produced by FESTO. The PAM is a type of pneumatic actuator and has many advantages over conventional cylinder-type pneumatic actuators. It is frictionless, and it has a high force to weight ratio [25]. However, the dynamics of a PAM are complicated due to intrinsic non-linear characteristics. A range of research studies have been done to investigate PAM dynamic behaviour [26-28]. The modelling of the unit cell is described in Section 4, and a bang-bang controller is shown for the control of position and force of the unit cell in simulation. Experimental results are shown in Section 5, and the conclusions are drawn in Section 6.

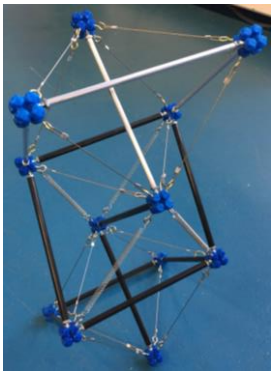

Figure 1. Model of a class 3 tensegrity structure.

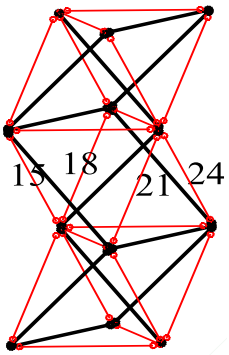

Figure 2. Unactuated example 3-unit-cell tensegrity structure with finite node dimensions in isometric view.

2. Example actuated structure

This section demonstrates the form-finding calculation for an actuated 3-unit-cell tensegrity structure by using an iterative approach. To find the equilibrium state, node positions are continuously updated through iterations until the resultant force at each node is zero (if possible). For a physically realizable structure, struts cannot meet at a point, and thus each node has a finite size with some separation between the ends of the members meeting at the node. This feature is included in the form-finding algorithm. Details of the approach are in [29]. Figure 2 and 3 depict the equilibrium state of the example tensegrity at its unactuated position. Cables are shown as thin lines and struts are bold lines. There are 33 elements in the structure of which elements 1 to 13 are struts. It is essentially the physical model as shown in Figure 1.

Tensile members of the example structure can be controlled antagonistically to achieve three types of motion which will be named bending, shear and twisting deformation. The control can also change the pre-stressed level of the structure. A set of actuation examples is illustrated in Figure 4. The actuation is realised by controlling the lengths of members 15, 18, 21 and 24 in the middle unit cell. The top view in Figure 4 shows the structural equilibrium state when members 15 and 18 are contracted by 15% and members 21 and 24 extended by 20% of their original lengths. This causes a bending deformation of the structure. The front view in Figure 4 is an example of structural shear deformation achieved by contracting members 15 and 24 and extending members 18 and 21. The twisting motion in Figure 4 results from the contraction of members 15 and 21 and the extension of members 18 and 24.

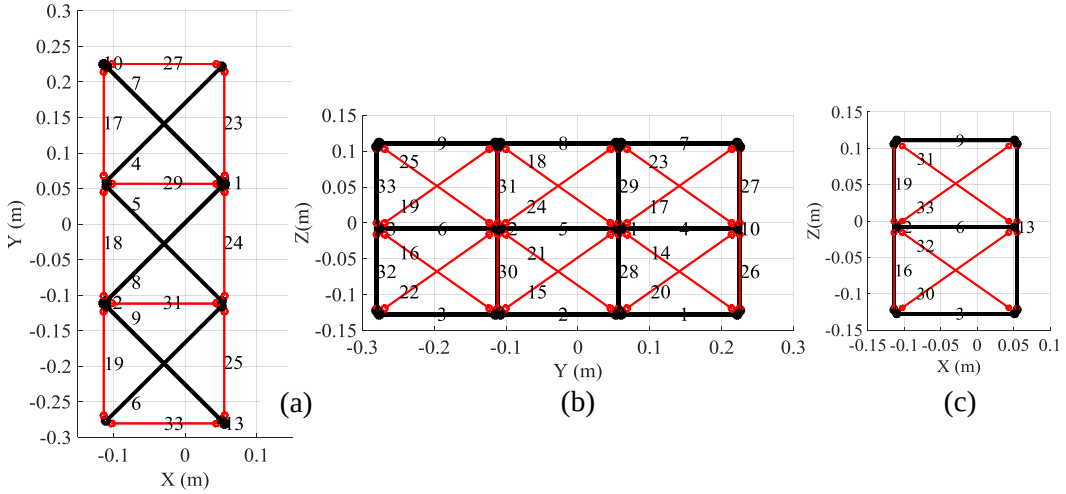

Figure 3. Unactuated example 3-unit-cell tensegrity structure with finite node dimensions in: **(a)** Top view, **(b)** Front view and **(c)** Side view.

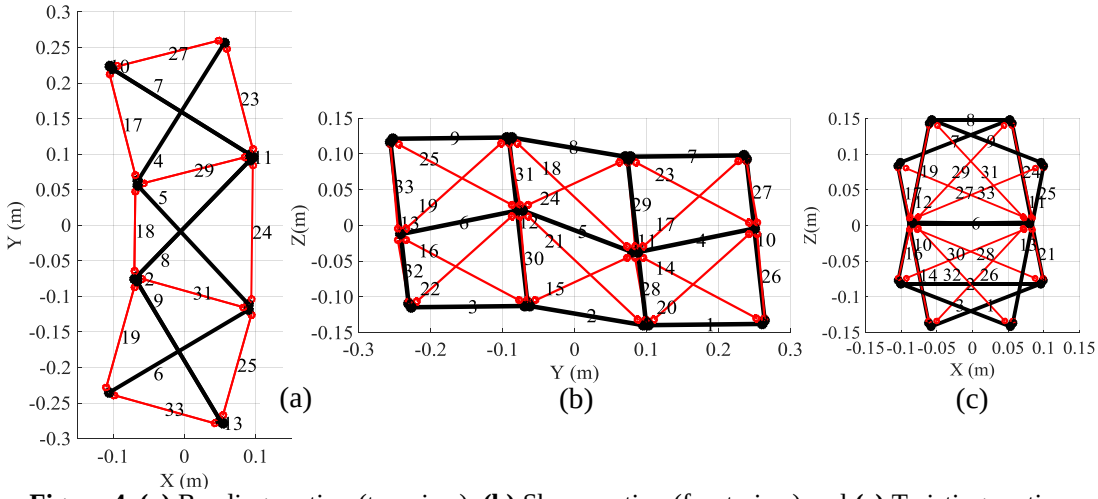

Figure 4. (a) Bending motion (top view), **(b)** Shear motion (front view) and **(c)** Twisting motion (side view).

3. Experimental system

The connection of one PAM is schematically illustrated in Figure 5. Each PAM is controlled by two modified 3/2 on-off solenoid valves. One solenoid valve is connected to a pressure source of 6 bar gauge pressure and is dedicated to pressurise the PAM, while the other solenoid valve is used to connect the PAM to atmosphere. The compressed air will be trapped in the PAM when both valves are off. A pressure transducer with a measuring range of 0-10 bar is connected at the PAM inlet in order to measure the pressure within the muscle. A draw-wire sensor with resolution of 0.1mm is used for the displacement measurement. The sensor is mounted on one end of the PAM with the wire being pulled out and attached at the other end. The measurements from the two devices are sent back to a host PC through an Arduino board with control and data acquisition functions. The setup allows a controller to be implemented as a Simulink model and the model parameters to be tuned on the host PC with the model running on the target Arduino board. The system provides real-time monitoring of the experimental signals which includes the pressure within the PAM, the displacement of the PAM, and

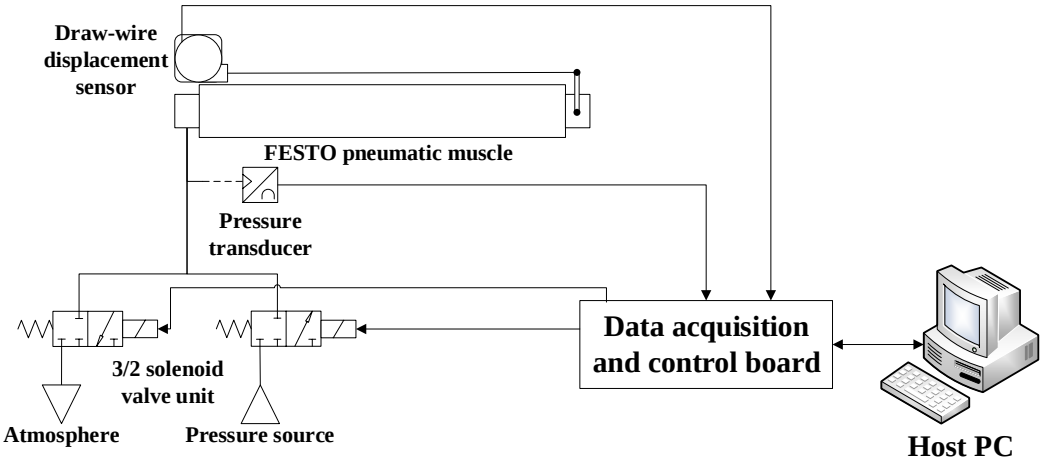

Figure 5. Schematic diagram for the connection of one PAM.

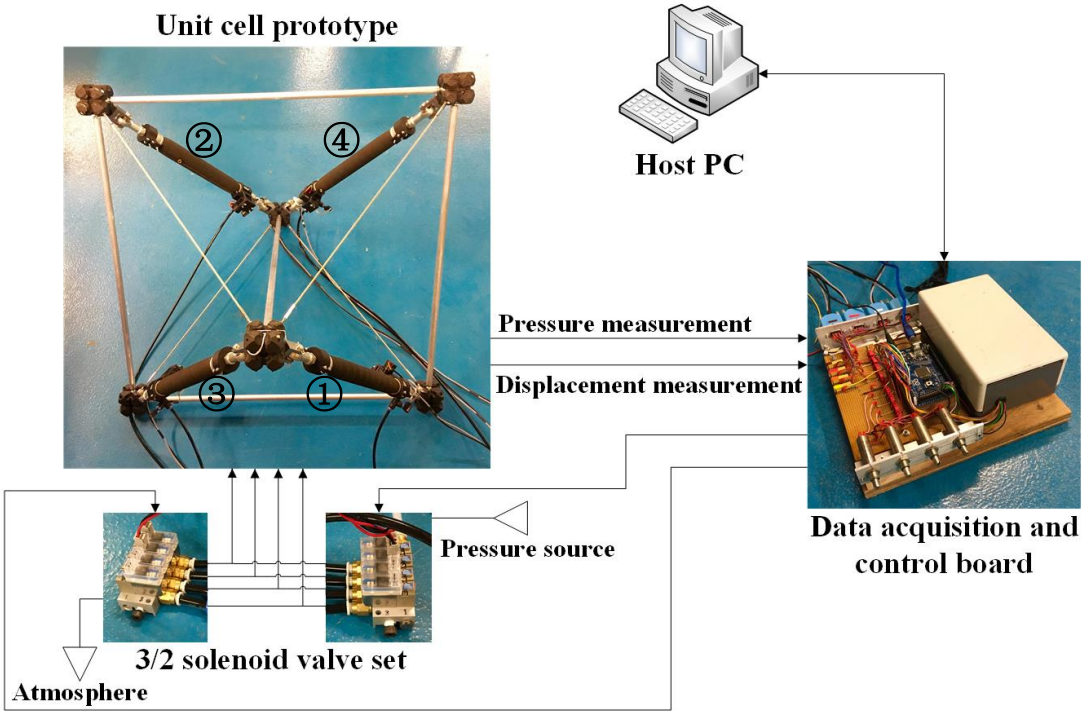

Figure 6. Experimental setup for the testing of the proposed tensegrity structure.

both the position and force demands and their corresponding feedbacks. The force feedback is estimated from PAM pressure and displacement as described in Subsection 4.1.

Figure 6 shows the arrangement of the experimental apparatus. Four PAMs are embedded into the tensegrity structure to actuate the structure antagonistically. The PAMs in this research are type DMSP-20-290N manufactured by FESTO. The muscle is constructed by wrapping the pressure-tight rubber tube with inextensible high-strength fibres. The fibres are orientated to create a rhomboidal pattern and are layered to build 3-D grid structure. When compressed air flows into the PAM, the tube expands in its circumferential direction, which generates a pulling force and a contraction movement in the longitudinal direction. The chosen PAM has an internal diameter of 20 mm and a nominal length of 290 mm when the muscle is unpressurised. The maximum permissible contraction of the PAM is 25% of its nominal length. Its operational range is between 0 and 6 bar gauge pressure.

The unit cell prototype is equivalent to the middle cell of the example structure in Figure 2 and is sized according to the mid-stroke position of the PAM, i.e. the length when the muscle contracts 12.5%. The prototype is a class 2 tensegrity structure and contains 13 members, of which 5 are struts (12.8 mm in diameter) made from aluminium alloy tube. The rest are tensile members, of which four are 3 mm stainless steel wires with swage studs at both ends and the remaining four are PAMs as mentioned previously. The lengths of each compressive member and tensile member are 614.4 mm and 524.8 mm, respectively.

4. Modelling and control

4.1 Modelling

This subsection presents mathematical models which are used to simulate the dynamic behaviour of the tensegrity prototype. The model incorporates the fluid dynamics, the empirical model of the PAM proposed in [28] and a 2-D lookup table to determine the tensile force of the PAM with a given pressure and displacement. The changes in pressure and volume of the PAM are dictated by the mass flow rate of the compressed air thus resulting in the change of tensile force and displacement of the muscle.

The dynamic behaviours of the airflow in the PAM are mainly governed by three equations [28]. They are the mass continuity equation of the compressed air, the ideal gas law, and the energy change equation for an open system. Three assumptions are made for the PAM model with the consideration of the actual circumstances. The 1st assumption is that air behaves like the ideal gas. The 2nd assumption is that pressure and temperature of the compressed air within the PAM are homogeneous. And the 3rd assumption is that heat transfer, kinetic energy and potential energy are neglected.

The mass continuity equation of the compressed air is as shown below. The net mass flow rate $\dot{m}$ within the control volume of the PAM could be expressed by the subtraction of the inflow rate $\dot{m}_{\text{in}}$ and the outflow rate $\dot{m}_{\text{out}}$.

$$\dot{m} = s\dot{m}_{\text{in}} - (1-s)\dot{m}_{\text{out}} \tag{1}$$

where s is either 0 or 1 which is depended on the actuation of the PAM. When s = 1, it means the compressed air flows into the muscle. When s = 0, it means the compressed air flows out of the muscle.

According to the ideal gas law, the equation of the state of the hypothetical ideal gas is:

$$PV = mR_{\text{s}}T \tag{2}$$

where P is the pressure of the air in the PAM, V is the volume of the air in the PAM, m is the mass of the air, R_{s} is the specific gas constant for the air, and T is the temperature of the air.

The energy change for an open system is as follows. Since the mass varies continuously, the net mass flow rate needs to be considered. The equation contains 3 forms of energy which are internal energy, kinetic energy and potential energy.

$$\frac{\mathrm{d}E_{\text{cv}}}{\mathrm{d}t} = \dot{Q} - \dot{W} + s\dot{m}_{\text{in}}\left(h_{\text{in}} + \frac{v_{\text{in}}^{\ 2}}{2} + gz_{\text{in}}\right) - (1-s)\dot{m}_{\text{out}}\left(h_{\text{out}} + \frac{v_{\text{out}}^{\ 2}}{2} + gz_{\text{out}}\right) \tag{3}$$

where E_{cv} is the energy of a control volume, $\dot{Q}$ is the rate of the heat exchange between the system and the surroundings, $\dot{W}$ is the rate of the work done by the system to the surroundings, h_{in} and h_{out} are the

specific enthalpies of the compressed air mass inflow and outflow from the muscle, v_{in} and v_{out} are the corresponding velocities, and z_{in} and z_{out} represent the altitude of the mass flow.

According to the first assumption, the air behaves like the ideal gas. Hence, the rate of the change in the internal energy, $\dot{U}$, could be written as a function that depends only on the temperature:

$$\dot{U} = \frac{\mathrm{d}(mc_{\mathrm{v}}T)}{\mathrm{d}t} \tag{4}$$

where $\dot{U}$ is the rate of the change in the internal energy and c_v is the specific heat at constant volume.

Mayer's relation gives the following relationship between the specific gas constant and specific heats for a perfect gas:

$$R_{\mathrm{s}} = c_{\mathrm{v}}(k-1) \tag{5}$$

$$k = \frac{c_{\mathrm{p}}}{c_{\mathrm{v}}} \tag{6}$$

where k is the heat capacity ratio and c_p is the specific heat at constant pressure.

Based on the second assumption, the following two relations could be derived:

$$h_{\mathrm{in}} = h_{\mathrm{out}} = c_{\mathrm{p}}T \tag{7}$$

$$\dot{W} = P\dot{V} \tag{8}$$

where $\dot{V}$ is the rate of change in volume of the PAM.

In accordance with the third assumption, the heat transfer and the changes in both the kinetic energy and the potential energy are neglected. So the energy change equation of the open system is, in fact, the energy change equation of the internal energy with $\dot{Q} = 0$, i.e. adiabatic process,

$$\dot{U} = -\dot{W} + [s\dot{m}_{\mathrm{in}}h_{\mathrm{in}} - (1-s)\dot{m}_{\mathrm{out}}h_{\mathrm{out}}] \tag{9}$$

By substituting equation (1), equation (2) and equations (4) – (8) into equation (9), the dynamic behaviour of the air pressure in the muscle is derived:

$$\dot{P} = -\frac{kP}{V}\dot{V} + \frac{kR_{\mathrm{s}}T}{V}\dot{m} \tag{10}$$

The dynamic behaviour of the PAM is mainly due to the net mass flow rate which results in the changes in pressure and volume of the PAM. The mass flow rate of the PAM is controlled by two solenoid valves and is governed by,

$$\dot{m} = C_{\mathrm{d}}C_{\mathrm{m}}A_{\mathrm{o}}f(P_{\mathrm{r}}) \tag{11}$$

$$f(P_{\mathrm{r}}) = \frac{P_{\mathrm{u}}}{\sqrt{T}}\begin{cases} 1 & \text{if} \quad P_{\mathrm{atm}}/P_{\mathrm{u}} \le P_{\mathrm{r}} \le P_{\mathrm{cr}} \\ C_{\mathrm{k}}[P_{\mathrm{r}}^{2/k} - P_{\mathrm{r}}^{(k+1)/k}]^{1/2} & \text{if} \quad P_{\mathrm{cr}} < P_{\mathrm{r}} \le 1 \end{cases} \tag{12}$$

$$P_{\mathrm{r}} = \frac{P_{\mathrm{d}}}{P_{\mathrm{u}}} \tag{13}$$

where C_d is the discharge coefficient, C_m is the mass flow parameter for the air, A_o is the opening area of the orifice, P_u is the valve upstream pressure, P_d is the valve downstream pressure, P_{atm} is the atmospheric pressure, P_{cr} is the critical pressure ratio, and C_k is a constant.

In the empirical model, the volume of the PAM is calculated by using the equation below as the PAM could maintain the cylindrical shape under different pressures:

$$V = \pi r_{\mathrm{e}}^{2}L \tag{14}$$

$$r_{\mathrm{e}}^{2} = a_1L^2 + a_0 \tag{15}$$

where L is the instantaneous length of the PAM, r_e is the equivalent radius of the PAM, a_1 and a_0 are the slope and intercept of the linear function which is derived through experiment.

Figure 7 is a 3-D graphic representation of the data in the 2-D lookup table. The data is derived from a FESTO product configuration software. The 2-D lookup table is used to represent the force output of the PAM at different displacements and pressures. The muscle can only exert tensile force, so the minimum force is 0. Based on the aforementioned equations in this subsection, a flow chart for the

calculation of the mathematical model is shown in Figure 8. The switching of the solenoid valves causes the variation in the net mass flow rate which in turn changes the pressure and the volume of the muscle and thus the tensile force in the muscle.

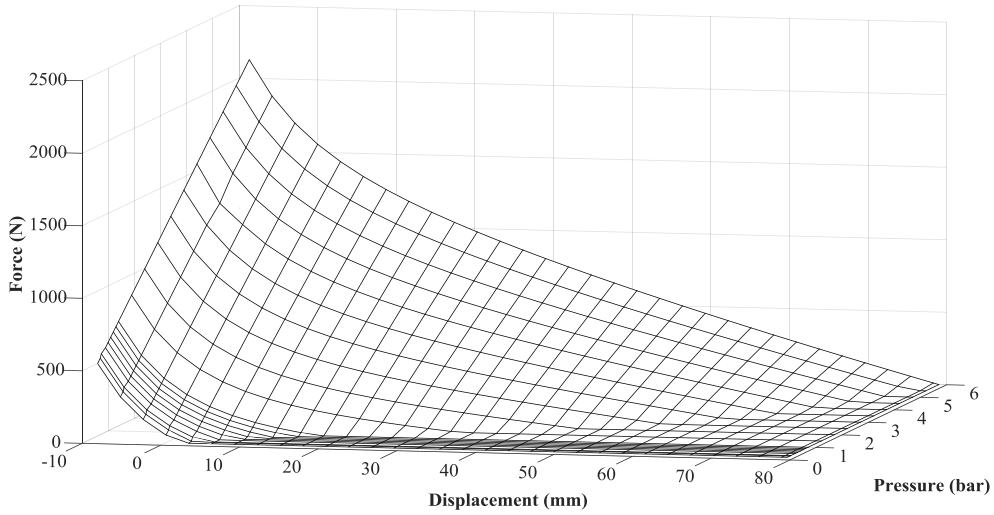

Figure 7. 3-D graphic representation of the data in the 2-D lookup table to represent the mechanical behaviours of the PAM.

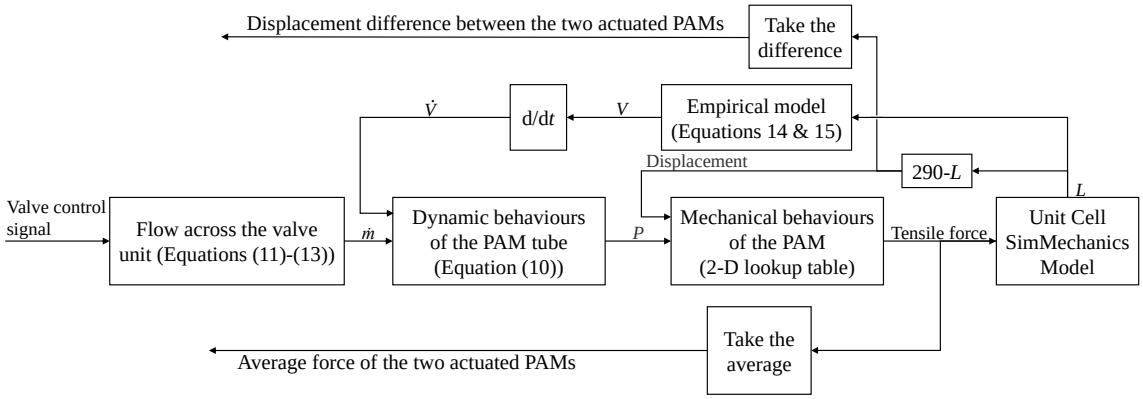

Figure 8. Flow chart for the calculation of the mathematical model in order to simulate the dynamic behaviours of the PAM.

4.2 Control strategy

A bang-bang controller (on-off controller) with both position and force control is adopted. The controller continuously switches the valves on and off until both the desired position and the pre-stress level are achieved. The strategy for the control of two PAMs is as shown in Figure 9. The controller contains a position loop and a force loop. As the actuators in the unit cell act against one another antagonistically, it is not feasible to individually control the position and the force of each PAM to reach the desired motion and the pre-stress level. The displacement of the structure is defined as the deviation of the structure from its unactuated state (neutral position). Hence, the position demand, in this paper, is simply a set of actuator position differences. When the structure deviates from its neutral position, the structure is no longer symmetrical, and thus the actuator forces will no longer be the same for an appropriately pre-loaded structure. So the force is controlled by taking the average of the actuator forces. The actuator forces are estimated from the measurements of pressures and displacements. For either loop, if the error is above its dead zone, an output of 1 will be generated. If the error is below its dead zone, the output will be -1. Within the dead zone the output is zero. The valve control signal for each PAM is created through the combination of the position and the force loop outputs. If the sum is positive, the high

pressure valve will be opened. If the sum is negative, the low pressure valve will be opened. Otherwise, both valves will be closed, i.e. the desired position and the pre-stress level are achieved. More details for the control of the whole structure are given in [29].

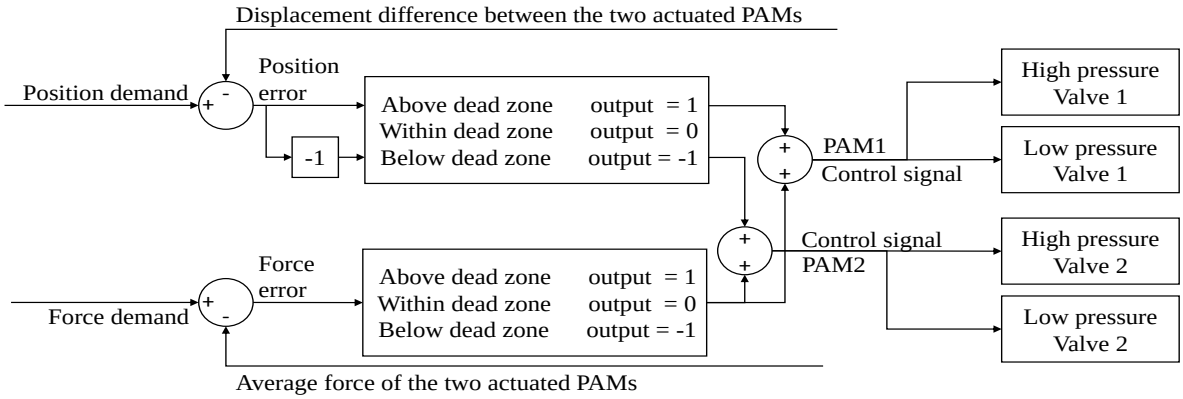

Figure 9. Bang-bang controller for the control of the motion and the pre-stressed level of the structure.

4.3 Simulation results

Two sets of simulation were carried out to investigate the dynamic behaviours of the unit cell according to the model and the controller given in Subsections 4.1 and 4.2. Four PAMs are modelled in Simulink, and these are embedded in a multi-body mechanical model of the unit cell implemented using SimMechanics (Figure 12). Table 1 lists the values of controller and model parameters for the simulation. The time step of the numerical integration is set to 0.001s. Only PAMs 1 and 2 are actuated (see Figure 6), while PAMs 3 and 4 are kept at constant pressure. Square wave demand signals of 10 and 40 mm amplitude used. For both simulations, the force demand is kept at 200 N. Initially, the lengths of the PAMs are the same and so are the pressures. Simulation results are presented in Figures 10 and 11.

Table 1. Values of controller and model parameters for the simulation of the unit cell.

Parameter	Description	Value	Unit
R_s	Specific gas constant	287	J/kgK
T	Ambient temperature	288.15	K
k	Heat capacity ratio	1.4	
C_d	Valve discharge coefficient	0.82	
C_m	Mass flow parameter for air	0.0405	
A_o	Maximum orifice area	0.32	mm^2
P_{cr}	Critical pressure ratio	0.528	
P_{atm}	Atmospheric pressure	101	kPa
C_k	Constant	3.864	
P_s	Supply pressure in absolute pressure	700	kPa
a_1	Slope	-0.005	
a_0	Intercept	6.735	
D_i	PAM initial displacement	36.25	mm
P_i	PAM initial pressure	300	kPa
T_c	Valve time constant	0.01	s
Z_p	Position dead zone	1	mm
Z_f	Force dead zone	2	N

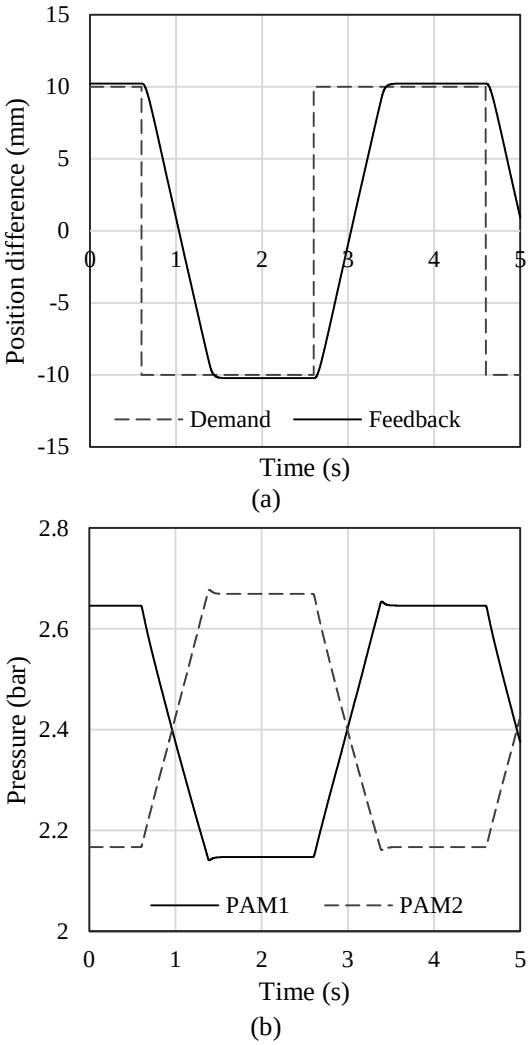

Figure 10. (a) Position demand of 10 mm and simulated position feedback, **(b)** Pressure results for the two actuated PAMs.

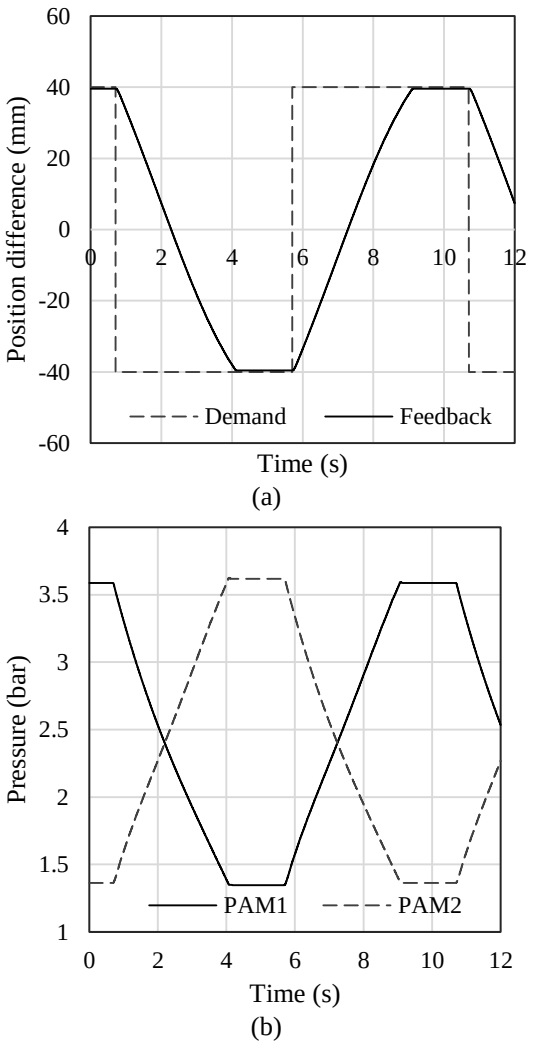

Figure 11. (a) Position demand of 40 mm and simulated position feedback, **(b)** Pressure results for the two actuated PAMs.

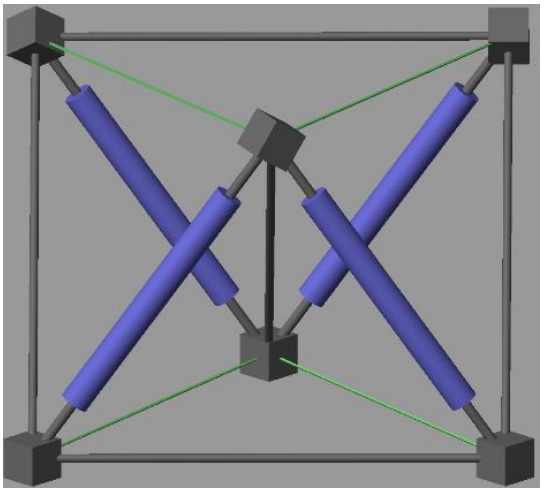

Figure 12. SimMechanics model of the unit cell.

5. Experimental results

Two sets of experiments were conducted to study the performance of the unit cell prototype by using the bang-bang control strategy and the experimental setup as discussed in Section 3. The pressure of the air supply is 6 bar gauge pressure, and the temperature in the laboratory is 15°C. The controller sample rate is 20 Hz, which means the controller will update the valve on-off signals every 0.05 s. The experimental settings are the same as the settings of the simulation for the purpose of comparison. During the experiments presented here, PAM 1 and 2 were actuated antagonistically while the remaining two were supplied with a pressure of 2 bar gauge pressure. Figures 13 and 14 show the measured motion of the unit cell with a square wave demand of 10 and 40 mm amplitude respectively. The force demand signal for both experiments is kept the same at 200 N. The results demonstrate that position control of the unit cell can be successfully achieved. However, the pressure and force deviations of the two PAMs are slightly different in the positive and negative directions, indicating that although the unit cell is designed to be symmetric, its assembly is not perfect which has resulted in slight asymmetry of the structure. Note that the average force is controlled well to be close to the 200N demand, but the individual actuator forces vary significantly as the structure moves away from its neutral position.

The experimental step responses are similar to the simulation results. However, the measured pressures show some differences from their corresponding simulation results. It can be seen that the pressure variation is greater in the experiments. This is likely to be due to the friction at the connections in the unit cell. In the simulation, the mechanical behaviour of each PAM is calculated from the 2-D lookup table through interpolation. The size of the data sample is limited. By using more points in the lookup table, the discrepancy between the experiment and the simulation may be reduced.

6. Conclusions

The proposed bang-bang controller can effectively actuate the prototype to achieve position control of the tensegrity structure, while maintaining the required pre-load. In terms of the simulation, the presented model of the unit cell replicates the motion and force dynamics of the prototype reasonably well. However, friction may be significant in the joints and this is not yet included in the model. A full non-linear model of the PAM will be used in the future to replace the 2-D lookup table in order to represent the characteristics of the muscle better. The next step in the research is to add another 2 unit cells to the existing one and control the 4 PAMs together to achieve bending, shear and twisting motion of the whole structure. This will help to validate the hypothesis that tensegrity structures are a viable concept for lightweight, high stiffness structures with actively controllable shape.

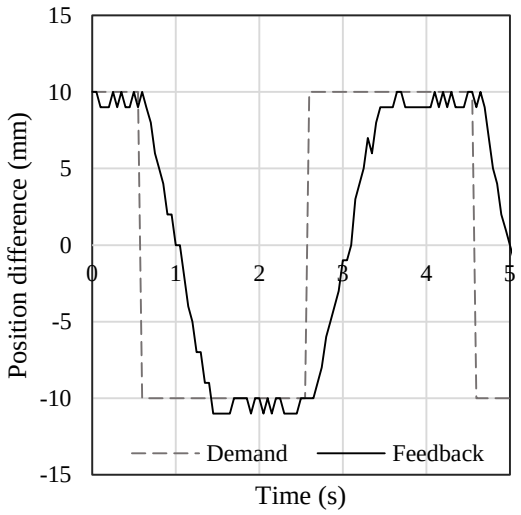

(a)

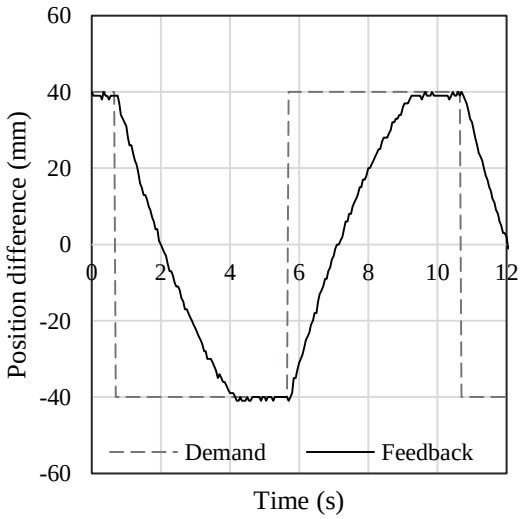

(a)

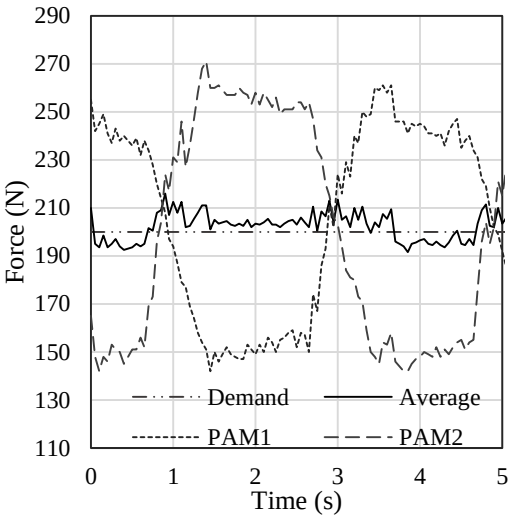

(b)

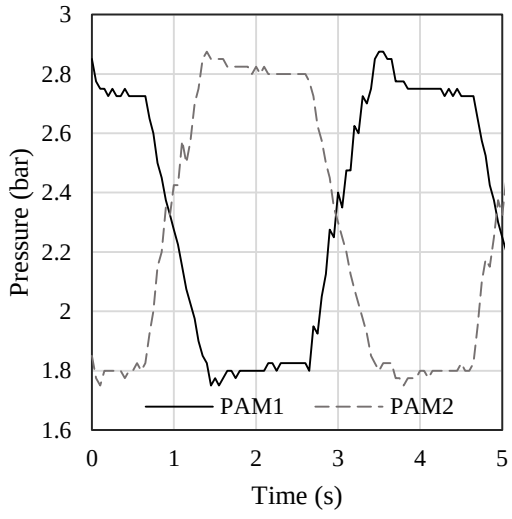

(c)

Figure 13. (a) Position demand of 10 mm and measured position feedback, **(b)** Force results for the two actuated PAMs, **(c)** Pressure results for the two actuated PAMs.

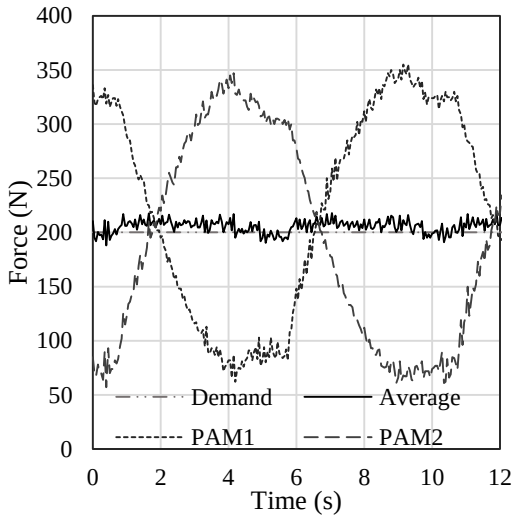

(b)

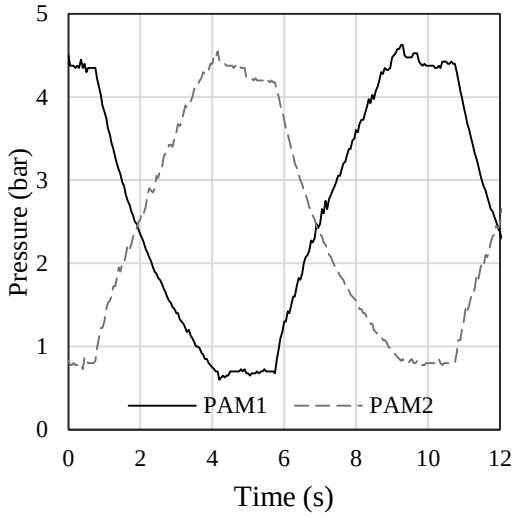

(c)

Figure 14. (a) Position demand of 40 mm and measured position feedback, **(b)** Force results for the two actuated PAMs, **(c)** Pressure results for the two actuated PAMs.

References

[1] Lawrence B and Padfield G D 2006 Flight handling qualities of the Wright brothers' 1905 Flyer 3 *Journal of Aircraft* **43**(5) 1307–16

[2] Weisshaar T A 2013 Morphing Aircraft Systems: Historical Perspectives and Future Challenges *Journal of Aircraft* **50**(2) 337–53

[3] Barbarino S, Bilgen O, Ajaj R M, Friswell M I and Inman D J 2011 A Review of Morphing Aircraft *J. Intell. Mater. Syst. Struct.* **22**(9) 823–77

[4] Thill C, Etches J, Bond I, Potter K and Weaver P 2008 Morphing skins *Aeronaut. J.* **112**(1129) 117–39

[5] Gern F H, Inman D J and Kapania R K 2005 Computation of actuation power requirements for smart wings with morphing airfoils *Aiaa J.* **43**(12) 2481–6

[6] Allen B Designing the 21st Century Aerospace Vehicle - Opening the Door to a New Era in Flight 22 Apr 2008 [cited 26 Jan 2016]; Available from: http://www.nasa.gov/centers/langley/news/factsheets/21stcentury.html

[7] Ingber D E 1997 Tensegrity: The architectural basis of cellular mechanotransduction *Annu. Rev. Physiol.* **59** 575–99
[8] Moored K W and Bart-Smith H 2007 The analysis of tensegrity structures for the design of a morphing wing *J. Appl. Mech.-Trans. ASME* **74**(4) 668–76
[9] Fuller R B 1962 Tensile-Integrity Structures U.S. Patent: 3 063 521
[10] Skelton R E and Oliveira M C 2009 *Tensegrity Systems* 1st ed (Boston: Springer US)
[11] Skelton R E, Adhikari R, Pinaud J P, Chan W L and Helton J W 2001 An introduction to the mechanics of tensegrity structures *Proc. of 40th IEEE Conf. on Decision and Control* (*Orlando*) vol 5 (New York: IEEE) pp 4254–9
[12] Benaroya H 1993 Tensile-Integrity Structures for the Moon *Applied Mechanics Reviews* **46**(6) 326
[13] Tibert A G and Pellegrino S 2002 Deployable tensegrity reflectors for small satellites *J. Spacecr. Rockets* **39**(5) 701–9
[14] Caluwaerts K, Despraz J, Iscen A, Sabelhaus A P, Bruce J, Schrauwen B and SunSpiral V 2014 Design and control of compliant tensegrity robots through simulation and hardware validation *J. R. Soc. Interface* **11**(98) 13
[15] Toklu Y C, Temur R, Bekdas G and Uzun F 2013 Space Applications of Tensegric Structures *Proc. of 6th Int. Conf. on Recent Advances in Space Technologies* (*Istanbul*) (New York: IEEE) pp 29-32
[16] Canadas P, Wendling-Mansuy S and Isabey D 2006 Frequency response of a viscoelastic tensegrity model: Structural rearrangement contribution to cell dynamics *J. Biomech. Eng.-Trans. ASME* **128**(4) 487–95
[17] Sultan C, Stamenovic D and Ingber D E 2004 A computational tensegrity model predicts dynamic rheological behaviors in living cells *Ann. Biomed. Eng.* **32**(4) 520–30
[18] Luo Y Z, Xu X, Lele T, Kumar S and Ingber D E 2008 A multi-modular tensegrity model of an actin stress fiber *J. Biomech.* **41**(11) 2379–87
[19] Zhang J Y, Guest S D and Ohsaki M 2009 Symmetric prismatic tensegrity structures. Part II: Symmetry-adapted formulations *International Journal of Solids and Structures* **46**(1) 15-30
[20] Zhang J Y, Guest S D, Connelly R and Ohsaki M 2010 Dihedral 'star' tensegrity structures *International Journal of Solids and Structures* **47**(1) 1-9
[21] Koohestani K and Guest S D 2013 A new approach to the analytical and numerical form-finding of tensegrity structures *International Journal of Solids and Structures* **50**(19) 2995-3007
[22] Koohestani K 2013 A computational framework for the form-finding and design of tensegrity structures *Mech. Res. Commun.* **54** 41-49
[23] Tran H C and Lee J 2013 Form-finding of tensegrity structures using double singular value decomposition *Eng. Comput.* **29**(1) 71-86
[24] Zhang L Y, Li Y, Cao Y P and Feng X Q 2014 Stiffness matrix based form-finding method of tensegrity structures *Eng. Struct.* **58** 36-48
[25] Tondu B 2012 Modelling of the McKibben artificial muscle: A review *J. Intell. Mater. Syst. Struct.* **23**(3) 225–53
[26] Shen X R 2010 Nonlinear model-based control of pneumatic artificial muscle servo systems *Control Eng. Practice* **18**(3) 311–7
[27] Pujana-Arrese A, Mendizabal A, Arenas J, Prestamero R and Landaluze J 2010 Modelling in Modelica and position control of a 1-DoF set-up powered by pneumatic muscles *Mechatronics* **20**(5) 535–52
[28] Wickramatunge K C and Leephakpreeda T 2013 Empirical modeling of dynamic behaviors of pneumatic artificial muscle actuators *ISA Trans.* **52**(6) 825–34
[29] Plummer A and Lai G 2015 New concepts for parallel kinematic mechanisms using fluid actuation *7th Int. Conf. on Fluid Power and Mechatronics (Harbin)*